J. Fluid Mech. (1992), *vol.* 237, *pp.* 649–669
Printed in Great Britain

Instabilities of the liquid and mushy regions during solidification of alloys

By M. GRAE WORSTER

Department of Engineering Sciences and Applied Mathematics *and* Department of Chemical Engineering, Northwestern University, Evanston IL 60208, USA

(Received 6 June 1991 and in revised form 4 September 1991)

The solidification of melts can be profoundly influenced by convection. In alloys, compositional convection can be driven by solute gradients generated as one component of the alloy is preferentially incorporated within the solid, even when the thermal field is stabilizing. In this paper, two modes of compositional convection during solidification from below are uncovered using a linear-stability analysis: one, which we shall call the 'mushy-layer mode', is driven by buoyant residual fluid within a mushy layer, or porous medium, of dendritic crystals; the other, which we shall call the 'boundary-layer mode' is associated with a narrow compositional boundary layer in the melt just above the mush–liquid interface. Either mode can be the first to become unstable depending on the thermodynamical and physical properties of the alloy. The marginally stable eigenfunctions suggest that the boundary-layer mode results in fine-scale convection in the melt above the mushy layer and leaves the interstitial fluid of the mushy layer virtually stagnant. In contrast, the mushy-layer mode causes perturbations to the solid fraction of the mushy layer that are indicative of a tendency to form chimneys, which are vertical channels of reduced or zero solid fraction that have been observed experimentally. Particular attention is focused on the mushy-layer mode and its dependence upon the thermodynamical properties of the alloy. The results of this analysis are used to make a number of interpretations of earlier experimental studies such as the observations that some systems are less prone to form chimneys and that the regions of melt in these systems evolve to supersaturated conditions, while the melt evolves to unsaturated conditions once chimneys have formed. In addition, good quantitative agreement is found between the results of the linear-stability analysis and the experimental results of Tait & Jaupart (1992) for the onset of the mushy-layer mode of convection.

1. Introduction

It is now commonly accepted that certain imperfections, called 'freckles', that are found in castings of metallic alloys are caused by some form of convection of the melt during solidification. Two types of compositional convection have been observed in laboratory experiments. In certain aqueous solutions, convection in the form of discrete plumes are observed to emanate from chimneys in a mushy layer of dendritic crystals. These chimneys are vertical channels of zero solid fraction that are strikingly similar to the freckles found in experimentally cast ingots of metallic alloys (Copley *et al.* 1970; Sarazin & Hellawell 1988). On the other hand, similar experiments using different aqueous solutions exhibit a visually different type of convection and fail to produce chimneys (Huppert 1990). It is not yet known what

key features distinguish these two classes of experiments. In particular, much attention is currently focused on the questions of when and how chimneys are formed, with the ultimate aim of producing castings that are free of freckles.

Chimneys have been most easily observed in the laboratory during the solidification from below of aqueous solutions of ammonium chloride. Consequently, such experiments have directed much of the current thinking in this field. The evolution of the solidification seems always to follow three stages (see, for example, Chen & Chen 1991 and Tait & Jaupart 1992). Initially, a fairly uniform layer of dendritic crystals forms on the cooled base of the experimental tank, and buoyant residual fluid, depleted of the ammonium chloride taken up by the crystals, rises convectively to form a layer of double-diffusive fingers. Some time later, a few isolated convective plumes are seen to rise much higher than the top of the layer of fingers. Eventually, a chimney or vent is observed beneath each plume extending through the crystal pile to the base of the tank. The plumes grow in number and strength and, as they do so, the double-diffusive, finger convection wanes. This rise in plume activity is followed by a third and final stage in which the number of chimneys declines.

The observed order of events (finger convection, followed by plumes, followed by chimneys) might lead one to suspect that the plumes are a more evolved form of the finger convection or that they are a direct consequence of the finger convection. Indeed, some support for this idea was provided by Hellawell (1987), who observed that chimneys could be induced by using a pipette to suck fluid vertically upwards from a region just above the top of the mushy layer. This suggested that fluid rising in double-diffusive fingers above the interface could provide a sufficient disturbance to initiate the formation of a chimney.

The present paper arrives at a somewhat different conclusion: that the fingers and the plumes are two independent modes of convection. These modes might interact but they can each be destabilized without the pre-existence of the other. One mode, which we shall call the mushy-layer mode, is driven by the compositional buoyancy within the mushy layer. The other is driven by the compositional buoyancy in a boundary layer that exists above and adjacent to the mush–liquid interface, and we shall call this the boundary-layer mode.

These two modes are analogous to those found by Chen & Chen (1988) in a porous layer underlying a fluid layer subject to a destabilizing, linear temperature gradient. In the present paper, the destabilizing buoyancy is provided by the compositional depletion associated with the growth of crystals from a binary mixture, the porous medium is the mushy layer of dendritic crystals, and the overlying fluid layer is the melt from which the crystals are growing. The motionless basic state that we shall study varies considerably with the thermodynamic properties and external parameters of the system, and we shall explore how these affect the onset and nature of convection.

The stability of similar systems has been investigated previously by Fowler (1985) and by Nandapurkar *et al.* (1989). Fowler (1985) studied a special limiting form of the governing equations in which only the mushy-layer mode can be identified and, since the solid fraction was asymptotically zero in the limit he investigated, there was no interaction between the convection and the solidification. Nandapurkar *et al.* (1989) solved the full set of governing equations numerically though they did not allow any perturbations to the solid fraction in their stability analysis and thereby suppressed any interaction between convection and solidification. In addition, they worked with dimensional variables and investigated only one set of physical parameters. As a

result, they did not encounter the mushy-layer mode and concluded that the system would only be unstable to convection above the mushy layer while the fluid in the interstices of the mushy layer would remain essentially stagnant.

In contrast to both these studies, we treat the mushy layer as a reacting porous medium whose permeability varies as the solid dendrites grow or dissolve within it. We shall discover how the convection affects the local solid fraction within the mushy layer and draw conclusions regarding the way in which chimneys are formed.

2. Governing equations

The system to be investigated is illustrated in figure 1. A binary alloy of composition C_0 and temperature T_∞ is solidified at a constant rate V, with the temperature at the horizontal position $z = 0$ held fixed at the eutectic temperature T_e in a frame moving with the solidification speed. A mushy layer extends from $z = 0$ upwards to $z = h(x, y, t)$, and lies beneath a semi-infinite region of melt in $z > h$, where h must be determined as part of the solution.

The full set of governing equations we shall investigate here are described in detail by Worster (1991). Here we start with a dimensionless form of the equations for the case in which the properties of the solid and liquid are assumed to be identical. The variables are scaled as follows. Fluid velocities are scaled with the prescribed solidification rate V, distances with the thermal-diffusion lengthscale $H = \kappa/V$, time with κ/V^2 and pressure with $\beta\Delta C\rho_0 g\kappa/V$, where the compositional scale ΔC is given by $C_0 - C_e$, and C_e is the eutectic concentration of the alloy. Here, κ is the thermal diffusivity, ρ_0 is a reference density, g is the acceleration due to gravity, and $\beta = \beta^* - \Gamma\alpha^*$, where α^* and β^* are the expansion coefficients for heat and solute respectively and Γ is the slope of the liquidus curve, which is assumed to be constant. Dimensionless variables for temperature and concentration are defined by

$$\theta = \frac{T - T_L(C_0)}{\Delta T}, \quad \Theta = \frac{C - C_0}{\Delta C},$$

where $\Delta T = \Gamma\Delta C = T_L(C_0) - T_e$, and T_L is the local liquidus temperature.

In the liquid region, $z > h(x, y, t)$, dimensionless equations for conservation of heat, solute and momentum in the moving frame are given by

$$\frac{\partial\theta}{\partial t} - \frac{\partial\theta}{\partial z} + \boldsymbol{U}\cdot\boldsymbol{\nabla}\theta = \nabla^2\theta, \tag{2.1}$$

$$\frac{\partial\Theta}{\partial t} - \frac{\partial\Theta}{\partial z} + \boldsymbol{U}\cdot\boldsymbol{\nabla}\Theta = \epsilon\nabla^2\Theta, \tag{2.2}$$

$$\frac{1}{\sigma}\left(\frac{\partial\boldsymbol{U}}{\partial t} - \frac{\partial\boldsymbol{U}}{\partial z} + \boldsymbol{U}\cdot\boldsymbol{\nabla}\boldsymbol{U}\right) = \nabla^2\boldsymbol{U} + R_T\theta\hat{\boldsymbol{z}} - R_C\left(\Theta\hat{\boldsymbol{z}} + \frac{\beta}{\beta^*}\boldsymbol{\nabla}p\right), \tag{2.3}$$

where $\epsilon = D/\kappa$ is the ratio of diffusivities of solute and heat, the Prandtl number $\sigma = \nu/\kappa$, and thermal and solutal Rayleigh numbers are given by

$$R_T = \frac{\alpha^*\Delta T g H^3}{\kappa\nu}, \quad R_C = \frac{\beta^*\Delta C g H^3}{\kappa\nu}.$$

Note that the equations are written in terms of the volume flux of fluid per unit area

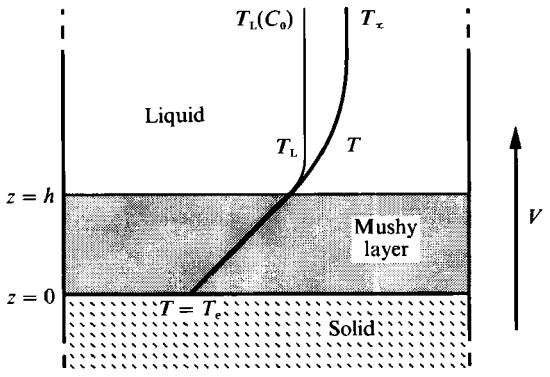

FIGURE 1. A schematic diagram representing the steady upwards solidification of an alloy at speed V. A mushy layer lies above a completely solid region, where the temperature is below the eutectic temperature, and below a completely liquid region. The temperature profile T is shown together with the profile of the local liquidus temperature T_L.

$\boldsymbol{U} = \chi \boldsymbol{u}$, where $\boldsymbol{u}$ is the actual fluid velocity and χ is the local liquid fraction. Clearly, in the completely liquid region $z > h$, the liquid fraction is equal to unity and $\boldsymbol{U} = \boldsymbol{u}$.

The boundary conditions to be applied to the variables in the liquid region are

$$\theta \to \theta_\infty, \quad \Theta \to 0, \quad \boldsymbol{U} \to 0 \quad (z \to \infty); \tag{2.4a–c}$$

$$\theta = \Theta, \quad \boldsymbol{n}\cdot\nabla\theta = \boldsymbol{n}\cdot\nabla\Theta, \quad [\boldsymbol{n}\cdot\boldsymbol{U}] = 0, \quad \boldsymbol{U} - \boldsymbol{n}\cdot\boldsymbol{U} = 0 \quad (z = h). \tag{2.5a–d}$$

The square brackets denote the jump in the enclosed quantity across the interface. Condition (2.5a) is the liquidus relationship applied at the mush–liquid interface, while (2.5b) is an expression of the condition of marginal equilibrium proposed by Worster (1986). Continuity of normal mass flux across the mush–liquid interface is expressed by condition (2.5c), and (2.5d) is the no-slip condition applied to the liquid adjacent to the interface with the mushy layer. Chen & Chen (1988) used the more general Beavers–Joseph condition in which there is a slip velocity that is proportional to the interfacial shear stress. We use the condition of no slip here for simplicity, so as not to introduce extra parameters into an already over-crowded set of governing equations. We note that the no-slip condition is an appropriate approximation if the scale of fluid motions is large in comparison with the pore size of the underlying porous medium and that its use here does not seem to lead to any qualitative differences from the results of Chen & Chen (1988).

Dimensionless equations for conservation of heat, solute and momentum in the mushy region, $0 < z < h$, are given by

$$\left(\frac{\partial}{\partial t} - \frac{\partial}{\partial z}\right)\left(\theta + \mathscr{S}\frac{\mathscr{C} - \xi}{\mathscr{C} - \theta}\right) + \boldsymbol{U}\cdot\nabla\theta = \nabla^2\theta, \tag{2.6}$$

$$\left(\frac{\partial}{\partial t} - \frac{\partial}{\partial z}\right)\xi + \boldsymbol{U}\cdot\nabla\theta = 0, \tag{2.7}$$

$$\frac{\boldsymbol{U}}{\Pi(\chi)} = -R_m(\nabla p + \theta\hat{\boldsymbol{z}}) \tag{2.8}$$

where

$$R_m = \frac{\beta\Delta C g \Pi^* H}{\kappa\nu}$$

is the Rayleigh number appropriate for the mushy layer, which is expressed in terms of a reference value Π^* of the permeability of the layer. We use Darcy's equation (2.8) here for simplicity and, again, to limit the number of parameters. Other authors (e.g. Nandapurkar *et al.* 1989) have favoured an extended Brinkman equation that includes effects of inertia and of deviatoric stresses within the mushy layer. Note that diffusion of solute has been ignored in (2.7) and that the liquidus relationship $\theta = \Theta$ is applied throughout the mushy layer. Here, the bulk composition $\xi = \chi\Theta + \phi\mathscr{C}$ is used as a dependent variable in place of either the liquid fraction χ or the solid fraction ϕ. The other dimensionless parameters introduced in these equations are a Stefan number

$$\mathscr{S} = \frac{\mathscr{L}}{c\Delta T},$$

where $\mathscr{L}$ is the latent heat of fusion and c is the specific heat, and a concentration ratio

$$\mathscr{C} = \frac{C_s - C_0}{\Delta C},$$

where C_s is the composition of the solid phase forming the dendrites.

The boundary conditions to be applied to the variables in the mushy region are

$$\theta = -1, \quad W = 0 \quad (z = 0); \tag{2.9a, b}$$

$$[\theta] = 0, \quad [\boldsymbol{n}\cdot\nabla\theta] = 0, \quad [p] = 0, \quad \xi = \Theta \quad (z = h). \tag{2.10a–d}$$

Conditions (2.10*a*) and (2.10*c*) express continuity of temperature and pressure across the mush–liquid interface, while conditions (2.10*b*) and (2.10*d*) are derived from expressions for the conservation of heat and solute once the condition of marginal equilibrium (2.5*b*) is taken into account.

3. Steady basic solution

The governing equations and boundary conditions presented in the preceding section admit a steady solution in which the temperature and composition depend only on the vertical coordinate z, the fluid velocity $\boldsymbol{U} = 0$ and the mush–liquid interface is at the fixed horizontal level $z = h_0$. This solution was presented by Worster (1991) and can be expressed as follows.

In the liquid region, $z > h_0$, the unperturbed temperature θ_0 and composition Θ_0 are given by the exponential profiles

$$\theta_0 = \theta_\infty + (\theta_1 - \theta_\infty)\,\mathrm{e}^{-(z-h_0)}, \tag{3.1}$$

$$\Theta_0 = \theta_1\,\mathrm{e}^{-(z-h_0)/\epsilon}, \tag{3.2}$$

with the interfacial temperature given by

$$\theta_1 = -\frac{\epsilon}{1-\epsilon}\theta_\infty. \tag{3.3}$$

In the mushy region, $0 < z < h_0$, the temperature/composition θ_0 is given implicitly by

$$z = \frac{\alpha - \mathscr{C}}{\alpha - \beta}\ln\left(\frac{\alpha+1}{\alpha-\theta_0}\right) + \frac{\mathscr{C}-\beta}{\alpha-\beta}\ln\left(\frac{\beta+1}{\beta-\theta_0}\right), \tag{3.4}$$

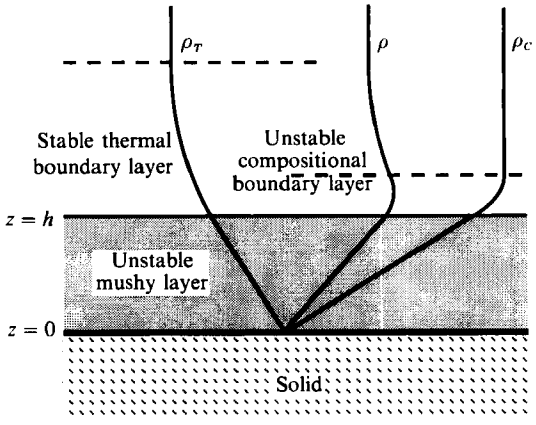

FIGURE 2. A schematic diagram showing the density variations due to temperature, ρ_T, and composition, ρ_C, and the total density field, ρ.

where

$$\alpha = A+B, \quad \beta = A-B, \quad A = \tfrac{1}{2}(\mathscr{C}+\theta_\infty+\mathscr{S}), \quad B^2 = A^2-\mathscr{C}\theta_\infty-\mathscr{S}\theta_i,$$

while the porosity χ_0 is given by

$$\chi_0 = \frac{\mathscr{C}-\theta_i}{\mathscr{C}-\theta_0}. \tag{3.5}$$

The unperturbed depth of the mushy layer h_0 is given by (3.4) with $\theta_0 = 0$.

The density fields associated with the temperature and concentration variations, as well as the total unperturbed density field, are illustrated in figure 2. We see that the thermal field is gravitationally stabilizing while the compositional field is destabilizing. We also see that most of the compositional variation is taken up by the mushy layer, where the fluid is relatively immobile, while there is a narrow compositional boundary layer in the more mobile liquid ahead of the mush–liquid interface. This picture led Worster (1991) to speculate that two different modes of convective behaviour are possible, one mode characterized by overturning of the fluid interior of the mushy layer on lengthscales typical of the depth of the mushy layer, and the other more or less confined to the boundary layer ahead of the mush–liquid interface with the fluid in the interstices of the mushy layer remaining essentially stagnant. This speculation is given substance by the following linear stability analysis.

4. Linear perturbation equations

The linear stability of the basic state just presented is investigated by introducing normal modes proportional to $e^{\omega t}e^{i\alpha x}$. These give rise to the following linearized equations and boundary conditions in which the variables θ, Θ and W now represent the disturbance amplitudes.

In the liquid region, $z > h$, the disturbance equations take the form

$$[D_z^2+(D_z-\omega)-\alpha^2]\,\theta = \theta_0' W, \tag{4.1}$$

$$[\epsilon D_z^2+(D_z-\omega)-\epsilon\alpha^2]\,\Theta = \Theta_0' W, \tag{4.2}$$

$$(D_z^2-\alpha^2)\,W = \Omega, \tag{4.3}$$

$$[D_z^2+((D_z-\omega)/\sigma)-\alpha^2]\,\Omega = \alpha^2(R_T\theta-R_C\Theta), \tag{4.4}$$

where $\mathrm{D}_z \equiv \mathrm{d}/\mathrm{d}z$, and a new variable Ω, representing the disturbance vorticity, has been introduced for convenience in (4.3). In the mushy region, $0 < z < h$,

$$\left\{\mathrm{D}_z^2+\left[1+\mathscr{S}\frac{\mathscr{C}-\theta_\mathrm{i}}{(\mathscr{C}-\theta_0)^2}\right](\mathrm{D}_z-\omega)+\frac{2\mathscr{S}\mathscr{C}\theta_0'}{(\mathscr{C}-\theta_0)^3}-\alpha^2\right\}\theta=\frac{\mathscr{S}\theta_0'}{(\mathscr{C}-\theta_0)^2}\xi+\left(1+\frac{\mathscr{S}}{\mathscr{C}-\theta_0}\right)\theta_0' W, \tag{4.5}$$

$$\left(\mathrm{D}_z^2-\frac{\Pi'(\chi_0)}{\Pi(\chi_0)}\frac{\mathscr{C}-\theta_\mathrm{i}}{(\mathscr{C}-\theta_0)^2}\theta_0'\,\mathrm{D}_z-\alpha^2\right)W=\alpha^2\Pi_0 R_\mathrm{m}\theta, \tag{4.6}$$

$$(\mathrm{D}_z-\omega)\xi=\theta_0' W. \tag{4.7}$$

These equations are subject to the linearized boundary conditions

$$\theta\to 0, \quad \Theta\to 0, \quad W\to 0, \quad \mathrm{D}_z W\to 0 \quad (z\to\infty); \tag{4.8}$$

$$\theta=\Theta, \quad \mathrm{D}_z\Theta-\mathrm{D}_z\theta=\frac{1-\epsilon}{\epsilon}\theta_0'\eta, \quad [W]=0, \quad \mathrm{D}_z W=0 \quad (z=h_0); \tag{4.9}$$

$$[\theta]=0, \quad [\mathrm{D}_z\theta]=-\frac{\mathscr{S}}{\mathscr{C}-\theta_\mathrm{i}}\theta_0'\eta, \quad \xi=\theta+\theta_0'\eta \quad (z=h_0); \tag{4.10}$$

$$\mathrm{D}_z W|_\mathrm{mush}=-\frac{\beta^* R_\mathrm{m}\Pi(1)}{\beta R_C}[\mathrm{D}\Omega=(\Omega+\alpha^2 W)/\sigma]_\mathrm{liquid} \quad (z=h_0); \tag{4.11}$$

$$\theta=0, \quad W=0 \quad (z=0); \tag{4.12}$$

where η is the perturbation to the position of the mush–liquid interface, i.e. $h(x,y,t)=h_0+\eta(x,y,t)$.

5. Marginal stability problem

In what follows, we seek only the onset of non-oscillatory instabilities. Indeed oscillatory instabilities are not expected to occur in the system being analysed since double-diffusive systems in which the slower diffusing component is unstably stratified, such as we have here, usually give way to direct modes of instability that lead to the formation of double-diffusive fingers. Accordingly, we set $\omega=0$ in the disturbance equations and seek their neutrally stable eigenfunctions.

Owing to the complexity of both the governing equations and the basic state, a numerical procedure was developed and utilized to determine the eigenvalues and eigenfunctions. Finding solutions is complicated by two features of this problem. One is that the melt occupies a semi-infinite domain and the other is that the basic state is only known implicitly via (3.4). The first difficulty can be dealt with by truncating the domain of integration at some finite distance above the solidification front (e.g. Coriell *et al.* 1980; Ng & Reid 1980). Instead, we introduce here a new technique, which is to use the basic-state temperature as the independent variable in the disturbance equations. Specifically we use the variable

$$\tau=\theta_\infty-\theta_0$$

as the independent variable so that the domain of integration runs from $\tau=0$ (corresponding to $z\to\infty$) to the eutectic front at $\tau=\tau_\mathrm{e}\equiv 1+\theta_\infty$. This approach should be found useful in many problems. Here, it has the added advantage that we avoid having to invert the transcendental equation (3.4).

The governing equations in the liquid region, $0 < \tau < \tau_i \equiv \theta_\infty/(1-\epsilon)$, thus become

$$(\tau^2 \mathrm{D}_\tau^2 - \alpha^2)\,\theta = \tau W, \tag{5.1}$$

$$(\epsilon\tau^2 \mathrm{D}_\tau^2 - (1-\epsilon)\,\tau \mathrm{D}_\tau - \epsilon\alpha^2)\,\Theta = \tau_i \left(\frac{\tau}{\tau_i}\right)^{1/\epsilon} W, \tag{5.2}$$

$$(\tau^2 \mathrm{D}_\tau^2 + \tau \mathrm{D}_\tau - \alpha^2)\,W = \Omega, \tag{5.3}$$

$$(\tau^2 \mathrm{D}_\tau^2 + (1-\sigma^{-1})\,\tau \mathrm{D}_\tau - \alpha^2)\,\Omega = \alpha^2 \mathscr{H} R_\mathrm{m}(\mathscr{A}\theta - (1+\mathscr{A})\,\Theta). \tag{5.4}$$

Here we have introduced new dimensionless parameters $\mathscr{H} = H^2/\Pi^*$ and $\mathscr{A} = \Gamma\alpha^*/\beta$, in place of $R_T = \mathscr{A}\mathscr{H} R_\mathrm{m}$ and $R_C = (1+\mathscr{A})\mathscr{H} R_\mathrm{m}$. In what follows, we fix $\mathscr{A}$ and $\mathscr{H}$ and use the Rayleigh number R_m as the bifurcation parameter representing the effects of gravity.

In the mushy region, $\tau_i < \tau < \tau_e \equiv \theta_\infty + 1$, the governing equations for marginal stability are

$$\left[\theta_0'^2 \mathrm{D}_\tau^2 + \frac{2\mathscr{S}\mathscr{C}\theta_0'}{(\mathscr{C}-\theta_0)^3} - \alpha^2\right]\theta = \frac{\mathscr{S}\theta_0'}{(\mathscr{C}-\theta_0)^2}\xi + \left(1 + \frac{\mathscr{S}}{\mathscr{C}-\theta_0}\right)\theta_0' W, \tag{5.5}$$

$$\left[\theta_0'^2 \mathrm{D}_\tau^2 + \left(1 + \left\{\mathscr{S} + \frac{\Pi'(\chi_0)}{\Pi(\chi_0)}\theta_0'\right\}\frac{\mathscr{C}-\theta_i}{(\mathscr{C}-\theta_0)^2}\right)\theta_0' \mathrm{D}_\tau - \alpha^2\right] W = \alpha^2 \Pi_0 R_\mathrm{m}\,\theta, \tag{5.6}$$

$$\mathrm{D}_\tau \xi = -W, \tag{5.7}$$

where

$$\theta_0' = \frac{(\alpha+\tau-\theta_\infty)(\beta+\tau-\theta_\infty)}{\mathscr{C}+\tau-\theta_\infty}. \tag{5.8}$$

Equations (5.1)–(5.8) are subject to the boundary conditions

$$\theta = 0, \quad \Theta = 0, \quad W = 0, \quad \mathrm{D}_\tau W = 0 \quad (\tau = 0); \tag{5.9}$$

$$\theta = \Theta, \quad \mathrm{D}_\tau\theta - \mathrm{D}_\tau\Theta = \frac{1-\epsilon}{\epsilon}\eta, \quad [W] = 0, \quad \mathrm{D}_\tau W = 0 \quad (\tau = \tau_i); \tag{5.10}$$

$$[\theta] = 0, \quad \mathrm{D}_\tau\theta|_\mathrm{mush} = \mathrm{D}_\tau\theta|_\mathrm{liquid} - \frac{\mathscr{S}}{\mathscr{C}-\theta_i}\eta, \quad \xi = \theta + \tau\eta \quad (\tau = \tau_i); \tag{5.11}$$

$$\mathrm{D}_\tau W|_\mathrm{mush} = -\frac{\Pi(1)}{\mathscr{H}}[\mathrm{D}_\tau\Omega - \sigma^{-1}(\Omega + \alpha^2 W)/\tau]_\mathrm{liquid} \quad (\tau = \tau_i); \tag{5.12}$$

$$\theta = 0, \quad W = 0 \quad (\tau = \tau_e). \tag{5.13}$$

Equations (5.1)–(5.4) have a regular singular point at $\tau = 0$. It is therefore helpful to write $(\theta, \Theta, W, \Omega) = \tau^m(\tilde\theta, \tilde\Theta, \tilde W, \tilde\Omega)$, where m is a root of the indicial equation, and to use the numerical procedure to solve for the analytic functions $(\tilde\theta, \tilde\Theta, \tilde W, \tilde\Omega)$. The equations solved numerically in the liquid region are thus

$$(\tau^2 \mathrm{D}_\tau^2 + 2m\tau \mathrm{D}_\tau + m^2 - m - \alpha^2)\,\tilde\theta = \tau\tilde W, \tag{5.14}$$

$$(\epsilon\tau^2 \mathrm{D}_\tau^2 + (2m\epsilon + \epsilon - 1)\,\tau \mathrm{D}_\tau + \epsilon m^2 - m - \epsilon\alpha^2)\,\tilde\Theta = \tau_i \left(\frac{\tau}{\tau_i}\right)^{1/\epsilon}\tilde W, \tag{5.15}$$

$$(\tau^2 \mathrm{D}_\tau^2 + (2m+1-\sigma^{-1})\,\tau \mathrm{D}_\tau + m^2 - m\sigma^{-1} - \alpha^2)\,\tilde\Omega = \alpha^2 \mathscr{H} R_\mathrm{m}(\mathscr{A}\tilde\theta - (1+\mathscr{A})\,\tilde\Theta), \tag{5.16}$$

$$(\tau^2 \mathrm{D}_\tau^2 + (2m+1)\,\tau \mathrm{D}_\tau + m^2 - \alpha^2)\,\tilde W = \tilde\Omega. \tag{5.17}$$

Four linearly independent solutions to these governing equations exist that satisfy the boundary conditions at $\tau = 0$ corresponding to values of m given by

$$m_1 = \tfrac{1}{2}(1+(1+4\alpha^2)^{\frac{1}{2}}), \quad m_2 = \tfrac{1}{2}(\epsilon^{-1}+(\epsilon^{-2}+4\alpha^2)^{\frac{1}{2}}),$$
$$m_3 = \tfrac{1}{2}(\sigma^{-1}+(\sigma^{-2}+4\alpha^2)^{\frac{1}{2}}), \quad m_4 = \alpha.$$

When m is equal to m_i, the corresponding values of $(\tilde{\theta}, \tilde{\Theta}, \tilde{\Omega}, \tilde{W})$ at $\tau = 0$ are given by the ith row of

i	$\tilde{\theta}$	$\tilde{\Theta}$	$\tilde{\Omega}$	$\tilde{W}$
1	1	0	$\dfrac{\alpha^2 R_T}{(m^2-\sigma^{-1}m-\alpha^2)}$	$\dfrac{\alpha^2 R_T}{(m^2-\sigma^{-1}m-\alpha^2)(m^2-\alpha^2)}$
2	0	1	$\dfrac{-\alpha^2 R_C}{(m^2-\sigma^{-1}m-\alpha^2)}$	$\dfrac{-\alpha^2 R_C}{(m^2-\sigma^{-1}m-\alpha^2)(m^2-\alpha^2)}$
3	0	0	1	$\dfrac{1}{m^2-\alpha^2}$
4	0	0	0	1

while, for each value of m, a Taylor expansion of the governing equations about $\tau = 0$ gives the following values for the first two derivatives of the dependent variables at $\tau = 0$:

$$\mathrm{D}_\tau\tilde{\theta} = \frac{\tilde{W}}{m^2+m-\alpha^2}, \qquad \mathrm{D}_\tau^2\tilde{\theta} = \frac{2\mathrm{D}_\tau\tilde{W}}{m^2+3m+2-\alpha^2};$$

$$\mathrm{D}_\tau\tilde{\Theta} = 0, \qquad \mathrm{D}_\tau^2\tilde{\Theta} = 0;$$

$$\mathrm{D}_\tau\tilde{\Omega} = \frac{\alpha^2 R_T\,\mathrm{D}_\tau\tilde{\theta}}{m^2+m(2-\sigma^{-1})+1-\sigma^{-1}-\alpha^2}, \qquad \mathrm{D}_\tau^2\tilde{\Omega} = \frac{\alpha^2 R_T\,\mathrm{D}_\tau^2\tilde{\theta}}{m^2+m(4-\sigma^{-1})+4-2\sigma^{-1}-\alpha^2};$$

$$\mathrm{D}_\tau\tilde{W} = \frac{\mathrm{D}_\tau\tilde{\Omega}}{m^2+2m+1-\alpha^2}, \qquad \mathrm{D}_\tau^2\tilde{W} = \frac{\mathrm{D}_\tau^2\tilde{\Omega}}{m^2+4m+4-\alpha^2}.$$

These expressions allow numerical evaluation of (5.14)–(5.17) to be started from asymptotic expressions for the dependent variables near $\tau = 0$. For each value of m in turn, the governing equations are integrated from $\tau = 0$ to $\tau = \tau_1$. The dependent variables in the mushy layer at $\tau = \tau_1$ are then related to the dependent variables in the liquid by the expressions

$$\theta = \tau^m\tilde{\theta},$$

$$\eta = \frac{\epsilon}{1-\epsilon}\tau^m\left[\mathrm{D}_\tau\tilde{\theta}-\mathrm{D}_\tau\tilde{\Theta}+m\left(\frac{\tilde{\theta}-\tilde{\Theta}}{\tau}\right)\right],$$

$$\mathrm{D}_\tau\theta = \tau^m\mathrm{D}_\tau\tilde{\theta}+m\tau^{m-1}\tilde{\theta}-\frac{\mathscr{S}}{\mathscr{C}-\theta_i}\eta,$$

$$W = \tau^m\tilde{W},$$

$$\mathrm{D}_\tau W = -\frac{\Pi(1)}{\mathscr{H}}\tau^{m-1}[\tau\mathrm{D}_\tau\tilde{\Omega}+(m-\sigma^{-1})\tilde{\Omega}-\alpha^2\sigma^{-1}\tilde{W}],$$

$$\xi = \tau^m\tilde{\theta}+\tau\eta.$$

These values are used to start the numerical integration of (5.5)–(5.7) at $\tau = \tau_i$, which continues until $\tau = \tau_e$. The solutions thus evaluated will not, in general, satisfy all the boundary and interfacial conditions. The remaining boundary and interfacial conditions are therefore used to compute the residuals r_{ij} corresponding to index m_i, where

$$r_{i1} = \tau^{m_i}(\theta - \Theta) \quad (\tau = \tau_i),$$

$$r_{i2} = \tau^{m_i} \mathrm{D}_\tau \tilde{W} + m\tau^{m_i - 1}\tilde{W} \quad (\tau = \tau_i),$$

$$r_{i3} = \theta \quad (\tau = \tau_e),$$

$$r_{i4} = W \quad (\tau = \tau_e).$$

The determinant of the matrix (r_{ij}), $\mathscr{D} = \mathscr{D}(R_m, \alpha; \epsilon, \mathscr{H}, \mathscr{A}, \sigma, \mathscr{S}, \mathscr{C}, \theta_\infty)$, is then computed, and the Rayleigh number R_m is varied until the determinant is equal to zero. The corresponding solutions are eigenfunctions of the governing equations representing the marginally stable states of the system.

6. Results

We begin our study with the three principal thermodynamic parameters $\mathscr{S}, \mathscr{C}$, and θ_∞ all set to unity. The eigenvalue relationship $\mathscr{D}(R_m, \alpha; \epsilon, \mathscr{H}, \mathscr{A}, \sigma) = 0$ then specifies a marginal-stability curve $R_m(\alpha)$ for each choice of the dimensionless parameters $\epsilon, \mathscr{H}, \mathscr{A}$ and σ. We set the Prandtl number $\sigma = 10$ throughout, this being the appropriate order of magnitude for many aqueous solutions. To begin with, we set the buoyancy ratio $\mathscr{A} = 0$, which is appropriate for cases in which the temperature has little effect on the density of the fluid. This is a simplifying assumption that eliminates all double-diffusive effects from the system. In addition, we assume for the moment that the permeability of the mushy layer is uniform and hence set the dimensionless function $\Pi(\chi) \equiv 1$. The two remaining parameters are the inverse Lewis number $\epsilon = D/\kappa$, which is typically very small, and the parameter $\mathscr{H} = H^2/\Pi^*$, which can be thought of as the square of the ratio of the thermal lengthscale (on which the depth of the mushy layer principally depends) to the average spacing between dendrites within the mushy layer. This ratio is typically very large; indeed $\mathscr{H}$ being large is one of the fundamental hypotheses upon which the governing equations for the mushy layer are derived.

The first illustrative example is displayed in figure 3, which shows the marginal-stability curve for values of $\epsilon = 0.025$ and $\mathscr{H} = 10^5$. The system is convectively unstable to disturbances of wavenumber α whenever the Rayleigh number is greater than the value $R_m(\alpha)$ given by the marginal-stability curve. The striking property of this marginal curve is that it has two minima, corresponding to two distinct modes of convection with eigenfunctions illustrated in figure 4. There is an instability at a wavelength comparable to the depth of the mushy layer (with wavenumber $\alpha = 2.25$), which causes flow throughout the mushy layer and the liquid region, and another instability at wavelengths comparable to the depth of the compositional boundary layer ahead of the mush–liquid interface (with wavenumber $\alpha = 13.3$). This second mode of instability, which we call the boundary-layer mode, is characterized by the fact that it leaves the fluid within the interstices of the mushy layer essentially stagnant (figure 4*b*). As a consequence, it is characterized further by causing little perturbation to the solid fraction, in contrast to the mushy-layer mode which is associated with the solid-fraction perturbations shown in figure 5. We see

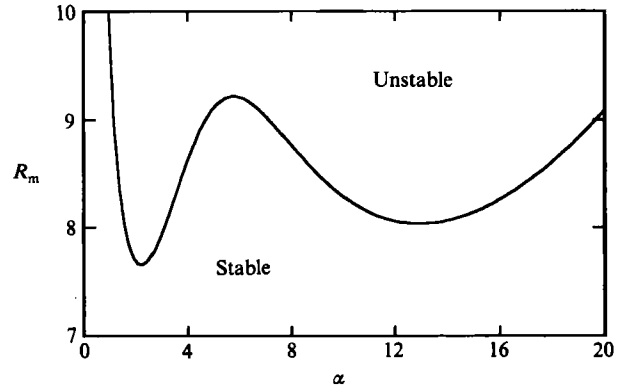

FIGURE 3. A representative marginal-stability curve with $\epsilon = 0.025$ and $\mathscr{H} = 10^5$. The two local minima correspond to the two different modes of convection discussed in the text.

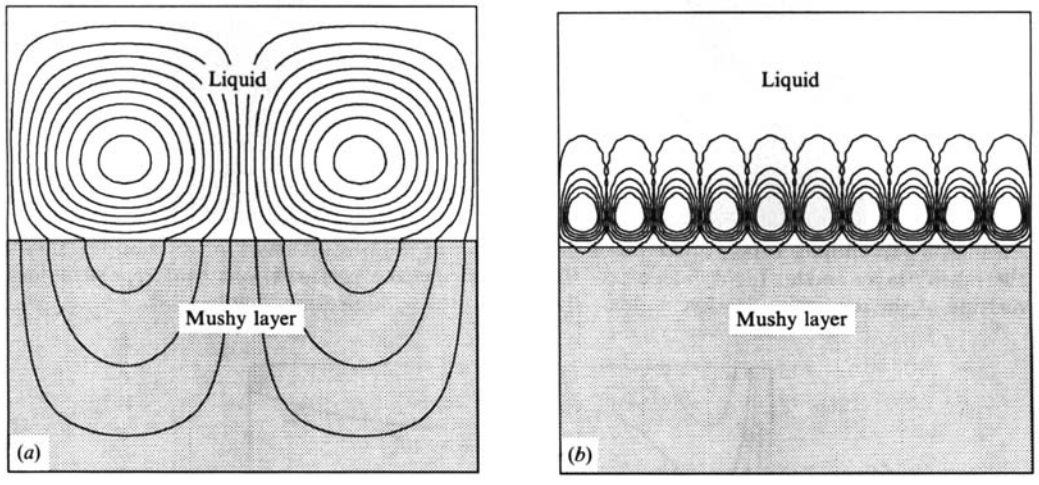

FIGURE 4. Streamlines for the two modes of convection corresponding to the local minima of the marginal-stability curve of figure 3.

that the mushy-layer mode is associated with an increase in the solid fraction at horizontal levels near the top of the layer in regions of upflow, which corresponds to an elevation of the mush–liquid interface there. In addition, there is a substantial decrease in the solid fraction in the interior of the mushy layer in regions of upflow. This is clearly indicative of a tendency to form chimneys; convective upflow results in a local decrease of the solid fraction and an elevation of the mush–liquid interface.

The relative stability of these two modes of convection, signified by the relative values of the local minima of the marginal-stability curve, varies considerably with the magnitudes of the parameters $\mathscr{H}$ and ϵ. An alternative interpretation of the parameter $\mathscr{H}$ is as a measure of the relative mobility of fluid in the melt region to that in the mushy layer. Therefore, increasing $\mathscr{H}$ causes the melt region to become more unstable relative to the mushy layer, as shown by the curves in figure 6. This figure also shows that either mode can be the most unstable depending on the parameters of the system.

The principal effect of varying ϵ is to change the thickness of the compositional boundary layer ahead of the mush–liquid interface relative to the depth of the mushy layer. As ϵ decreases, the thickness of the compositional boundary layer decreases,

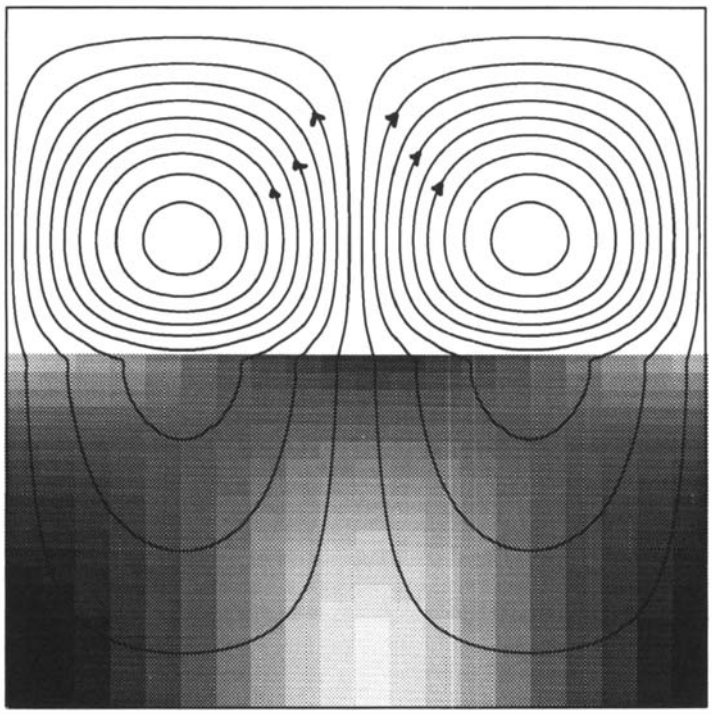

FIGURE 5. Streamlines superimposed on a density plot of the perturbation to the solid fraction in the mushy-layer mode. Light regions correspond to negative perturbations that represent local melting of the dendrites. Darker regions show where the solidification is enhanced.

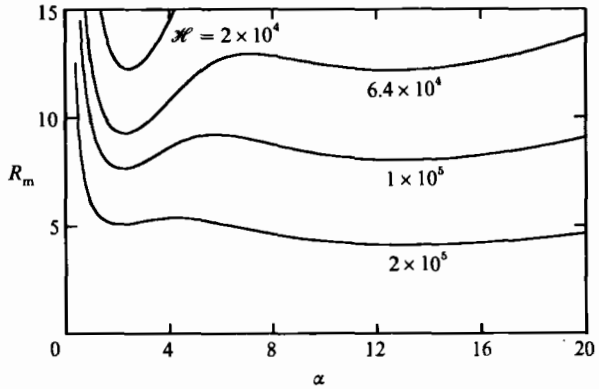

FIGURE 6. Marginal-stability curves for various values of $\mathscr{H}$ with $\epsilon = 0.025$ held fixed. Increasing $\mathscr{H}$ destabilizes the system overall and, in particular, destabilizes the boundary-layer mode relative to the mushy-layer mode.

which causes the local compositional Rayleigh number of the boundary layer (based on its thickness) to decrease proportionally to ϵ^3. The variation with ϵ of the minima corresponding to the two modes of convection is shown in figure 7. This variation is similar to that found by Chen & Chen (1988) as they varied the relative thickness of a liquid layer above a porous medium between impermeable walls. As ϵ decreases, the local minimum of the marginal-stability curve associated with the boundary-layer mode moves simultaneously to larger wavenumber and larger critical Rayleigh numbers.

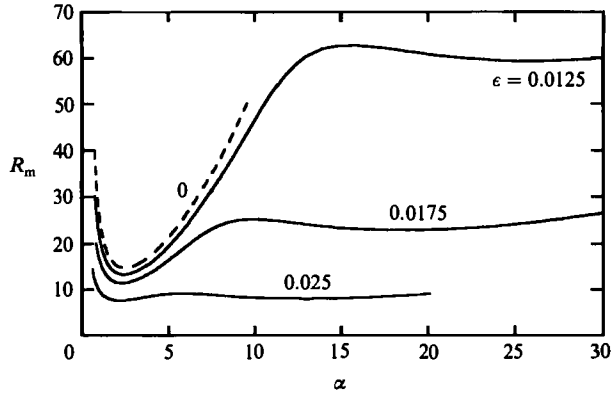

FIGURE 7. Marginal-stability curves for various values of ϵ with $\mathscr{H} = 10^5$ held fixed. Decreasing ϵ, decreases the thickness of the compositional boundary layer and causes the boundary-layer mode to be stabilized. The dashed curve was computed from the asymptotic form of the governing equations in the limit $\epsilon \to 0$.

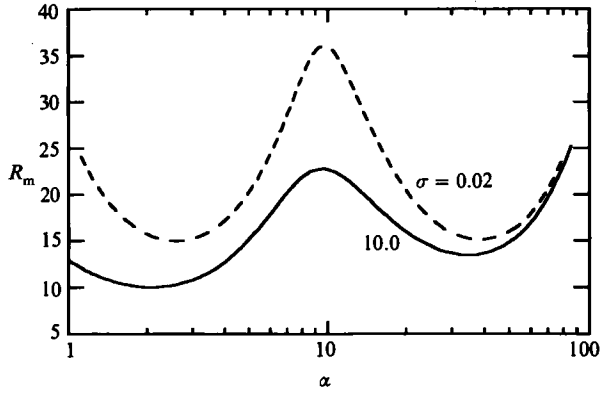

FIGURE 8. Marginal-stability curves for two different values of the Prandtl number σ, with $\epsilon = 10^{-2}$ and $\mathscr{H} = 10^6$: $\sigma = 10$ is an appropriate magnitude for many aqueous solutions, while $\sigma = 0.02$ is appropriate for metallic alloys.

Metallic alloys, which are of commercial interest, have Prandtl numbers that are much smaller than the aqueous solutions that are convenient for laboratory study. It is therefore important to consider the effect of the Prandtl number σ on the stability of these solidifying systems. In Bénard convection, the marginal stability curve is independent of σ, which affects only the growth rate of disturbances. In systems such as the one presently being studied, in which the velocity in the basic state is non zero (here by virtue of the moving reference frame), any vorticity generated by buoyancy is advected by this velocity field as well as being diffused. The inverse Prandtl number σ^{-1} measures the strength of this advection relative to diffusion, as can be seen from (4.4). Therefore, the smaller the Prandtl number, the larger is the advection of vorticity towards the solid boundary, which acts as a sink of vorticity by virtue of the no-slip condition. Thus systems with smaller Prandtl numbers tend to be more stable, as indicated by figure 8, which shows marginal-stability curves for two different values of σ. Note that σ is typically much larger than ϵ in physical systems, so it is not appropriate to consider smaller values of σ given the value of $\epsilon = 10^{-2}$ used to calculate the curves shown in this figure. A second role played by the Prandtl number in the present system is through the interfacial condition on the pressure field (4.11). This shows that decreasing σ tends to inhibit

the vertical velocity through the mush–liquid interface, which has a stabilizing effect on the mushy-layer mode as well as lessening the interaction between the two modes of convection. This latter effect is indicated by the greater relative height of the separating maximum at $\alpha \approx 10$ in figure 8. This figure illustrates further that the two modes are widely separated when ϵ is small. The equations are also very stiff in this limit, so it is convenient to rescale them appropriately for each mode and to investigate each separately.

The governing equations have so far been scaled with respect to the thermal-diffusion length and arranged such that R_m is employed as the principal bifurcation parameter. This is convenient for the study of the mushy-layer mode but not particularly appropriate for the boundary-layer mode. For that mode, it is better to consider a local compositional Rayleigh number $R_{\delta C} = \epsilon^3 \mathscr{H} R_m$ based on the thickness of the compositional boundary layer, the density contrast across it and the solutal diffusion coefficient. Then, for all the values of ϵ and $\mathscr{H}$ investigated, the critical value of $R_{\delta C}$ for the onset of the boundary-layer mode has been found to be between about 10 and 15. This is consistent with the values of the critical Rayleigh number determined by Hurle, Jakeman & Wheeler (1983) for compositional convection above a planar interface solidifying at a constant rate, which gives support to the idea that, at least when ϵ is small, the boundary-layer mode is largely insensitive to the mushy layer. With this assumption, one expects that increasing the buoyancy ratio $\mathscr{A}$ from zero will give rise to essentially the same double-diffusive modes of convection in the liquid region as have previously been studied extensively by previous authors (e.g. Coriell *et al.* 1980) and will not, therefore, be pursued here. We note only that increasing $\mathscr{A}$ will tend to stabilize the boundary-layer mode but slightly (Turner 1979).

For the remainder of this paper, we shall focus on the mushy-layer mode of instability which we have concluded is primarily responsible for the formation of chimneys. The mushy-layer mode can conveniently be studied in isolation by letting $\epsilon \to 0$ in the governing equations. This has the desirable effect of rendering the equations less stiff and thus more easily integrable numerically. We see from figure 7 that this procedure results in a very good approximation to the marginal-stability curve in the neighbourhood of the critical point of the mushy-layer mode when ϵ is small.

The nature and stability of the mushy-layer mode depends on the internal structure of the mushy layer, particularly on its permeability Π, which is a function of both its porosity χ and the morphology of the crystal interfaces within it. Many different empirical and semi-empirical relationships for Π have been determined for various porous media. One example is the Kozeny equation (Bear 1988) which gives $\Pi = c_0 \chi^3 / M^2$, where c_0 is a constant and M is the specific surface area of the phase boundaries per unit volume of the porous medium. This illustrates the general trends of all such formulae, namely that Π increases with the porosity and decreases with the specific surface area. In mushy layers, there are two opposing mechanisms affecting the specific surface area: morphological instabilities of the phase boundary give rise to the internal dendritic structure of the layer that increase the specific surface area, while Ostwald ripening serves to decrease the interfacial energy by decreasing the specific surface area. A prediction of the specific surface area is beyond the scope of the present theory but we can investigate the effect of varying porosity by choosing the simple dimensionless function

$$\Pi = \chi^3 \tag{6.1}$$

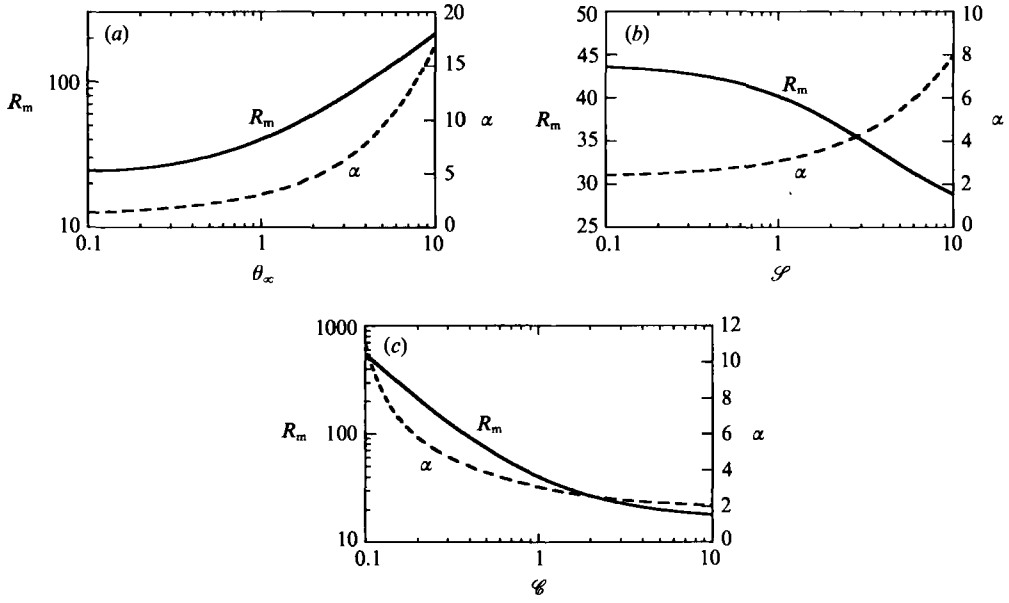

FIGURE 9. The variation of the critical Rayleigh number R_m and wavenumber α with the dimensionless parameters of the system. (*a*) The variation with θ_∞, while $\mathscr{S} = 1$ and $\mathscr{C} = 1$. (*b*) The variation with $\mathscr{S}$, while $\theta_\infty = 1$ and $\mathscr{C} = 1$. (*c*) The variation with $\mathscr{C}$, while $\mathscr{S} = 1$ and $\theta_\infty = 1$.

which is suggested by the form of the Kozeny equation with M held constant. We note that some previous authors (for example, Poirier 1988, and Nandapurkar *et al.* 1989) have used a formula in which $\Pi \propto \chi^3/(1-\chi)$, which is derived from the Kozeny equation for a regular array of cylinders. Such a formula, in which $\Pi \to \infty$ as $\chi \to 1$ is inappropriate when, as in this paper, the Darcy equation is used to describe the flow in the porous medium rather than the more general Brinkman equation.

With the permeability given by equation (6.1), the stability of the mushy-layer mode was investigated as the controlling thermodynamic parameters of the system are varied. The depth and internal structure of the mushy layer depends on the three principal thermodynamic parameters $\theta_\infty, \mathscr{S}$ and $\mathscr{C}$ as determined by (3.4) and (3.5), and discussed by Worster (1991).

The principal effect upon the basic, convectionless state of increasing the initial temperature of the melt θ_∞ is to decrease the unperturbed depth of the mushy layer (Worster 1991). Therefore the layer becomes more stable and the critical wavenumber increases as θ_∞ increases, as illustrated in figure 9(*a*).

The same behaviour might be expected when increasing the Stefan number $\mathscr{S}$ since this too decreases the unperturbed depth of the mushy layer. However, although the critical wavenumber increases with $\mathscr{S}$, as shown in figure 9(*b*), the same figure shows that the critical Rayleigh number decreases with increasing Stefan number. This behaviour might be attributable to the following physical effect. When fluid in the mushy layer is displaced upwards, it partly dissolves the dendrites it encompasses and thereby becomes denser. This is a stabilizing effect. Smaller values of the Stefan number (latent heat) result in more dissolution for the same perturbation, and thus cause the system to be more stable.

The critical Rayleigh number R_m varies most dramatically with $\mathscr{C}$, as shown in figure 9(*c*). As $\mathscr{C}$ increases, not only does the depth of the mushy layer increase but the porosity increases simultaneously. Thus the mushy-layer mode is greatly

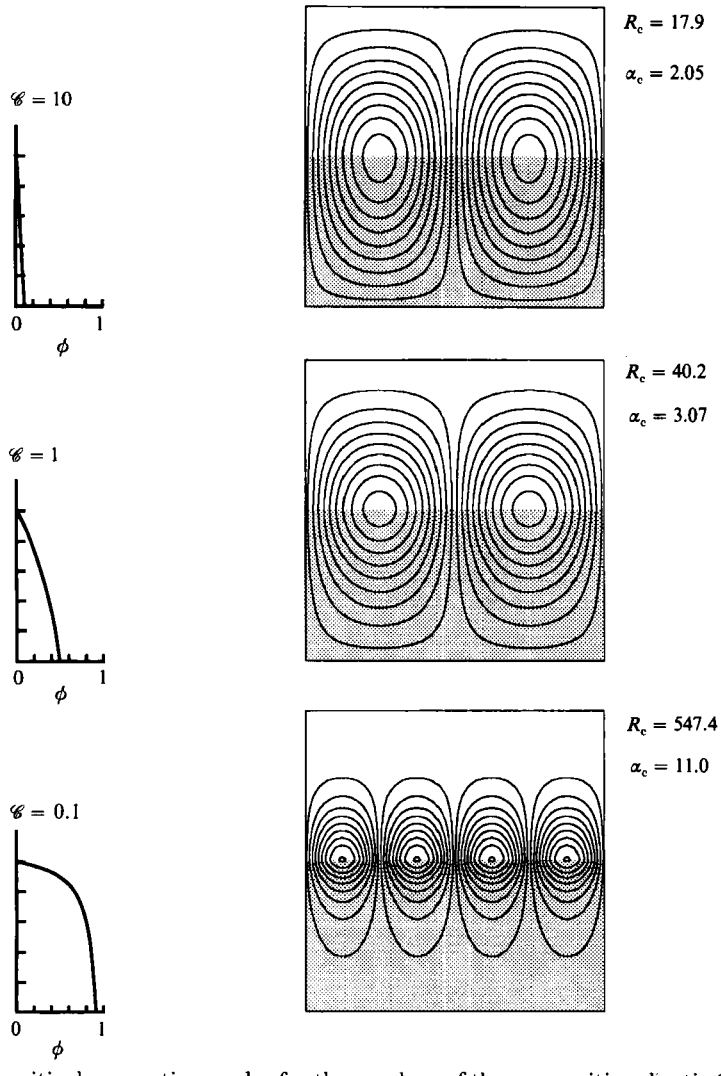

FIGURE 10. The critical convective modes for three values of the compositional ratio $\mathscr{C}$. Streamlines are shown alongside profiles of the solid fraction, ϕ, in the unperturbed state. Small values of $\mathscr{C}$ lead to large values of the solid fraction and to a localization of the flow to the upper regions of the mushy layer.

destabilized by increasing $\mathscr{C}$. Another effect of varying $\mathscr{C}$ is illustrated in figure 10, which shows the neutrally stable eigenfunctions alongside profiles of the solid fraction for three values of $\mathscr{C}$. When $\mathscr{C}$ is small, the porosity near the base of the layer is small, while the porosity always approaches unity at the top of the layer. Therefore, as $\mathscr{C}$ decreases, the flow becomes more confined to the upper part of the mushy layer, and this acts to stabilize the layer further.

We have defined the Rayleigh number R_m in terms of the thermal-diffusion lengthscale $H = \kappa/V$ and the permeability at the mush-liquid interface Π^*. These are both appropriate scales from a theoretical standpoint since each is an external parameter of the system. However, in laboratory experiments, it is often convenient to define a Rayleigh number in terms of the undisturbed depth of the mushy layer $h\kappa/V$ and the mean permeability of the layer $\Pi(\bar{\chi})\Pi^*$, where $\bar{\chi}$ is the mean porosity of the layer given by

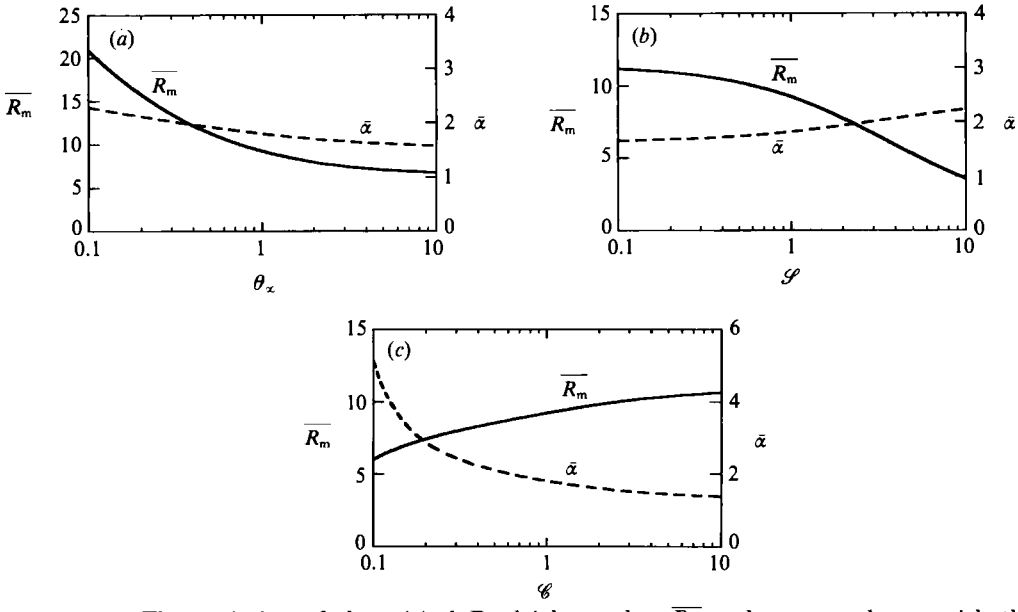

FIGURE 11. The variation of the critical Rayleigh number $\overline{R_m}$ and wavenumber $\bar{\alpha}$ with the dimensionless parameters of the system. These Rayleigh numbers and wavenumbers are scaled with respect to local properties of the undisturbed mushy layer. (*a*) The variation with θ_∞, while $\mathscr{S} = 1$ and $\mathscr{C} = 1$. (*b*) The variation with $\mathscr{S}$, while $\theta_\infty = 1$ and $\mathscr{C} = 1$. (*c*) The variation with $\mathscr{C}$, while $\mathscr{S} = 1$ and $\theta_\infty = 1$.

$$\bar{\chi} = \frac{1}{h}\int_0^h \chi_0(z)\,\mathrm{d}z, \tag{6.2}$$

which can be evaluated theoretically from (3.4) and (3.5) as

$$\bar{\chi} = \frac{1}{h}\frac{\mathscr{C}}{\alpha-\beta}\ln\left[\frac{\alpha(\beta+1)}{\beta(\alpha+1)}\right]. \tag{6.3}$$

Figure 11 shows graphs of the critical values of $\overline{R_m} = h\Pi(\bar{\chi})R_m$ and $\bar{\alpha} = h\alpha$ as they vary with the three controlling parameters θ_∞, $\mathscr{S}$ and $\mathscr{C}$. It can be seen that the critical wavenumber scaled on the depth of the mushy layer is almost constant, with a value of about 2, except for small values of $\mathscr{C}$ when convection is confined to the upper portions of the mushy layer.

7. Conclusions

The linear stability of a mushy layer to the onset of compositional convection has been analysed, and two modes of convection have been found. One, called the boundary-layer mode, is associated with the compositional buoyancy in a thin boundary layer above the mush–liquid interface and has a critical wavelength comparable to the thickness of that boundary layer. The other, called the mushy-layer mode, is driven by the buoyancy in the interior of the mushy layer and has a much larger critical wavelength, comparable to the full depth of the mushy layer. The boundary-layer mode was found to be almost independent of the details of the underlying mushy layer and to cause little perturbation of the solid fraction within the boundary layer. In contrast, the mushy-layer mode depends crucially on the

internal structure of the mushy layer and results in perturbations of the solid fraction that are indicative of a tendency to form chimneys. It was found that the Prandtl number has little effect on the stability of the system, though systems with smaller Prandtl numbers are slightly more stable, so that results of experiments with aqueous solutions will be indicative of the behaviour of metallic systems.

Experiments with transparent aqueous solutions have clearly demonstrated the existence of different forms of convection arising from mushy layers (Hellawell 1987; Huppert 1990; Chen & Chen 1991). In some systems, fine-scale convective motions are observed originating from near the mush–liquid interface. Indeed, such convection seems to be observed at some stage in all experiments and leads to a decrease of the temperature relative to the local liquidus temperature (Huppert 1990). On the other hand, in certain other experiments (notably those in which ammonium chloride is crystallized), this convection eventually gives way to a larger-scale convection that permeates the whole mushy layer, results in the formation of chimneys, and can cause the temperature of the liquid region to increase relative to the local liquidus.

In the light of the present analysis, the observed fine-scale convection can be interpreted as resulting from the boundary-layer mode of convective instability. The analysis has shown that this mode of convection does not penetrate the mushy layer and has no tendency (notwithstanding possible nonlinear effects) to produce chimneys. Kerr *et al.* (1990) have argued that non-equilibrium kinetic effects are important near the mush–liquid interface and cause local supercooling of the liquid. If this were taken into account, then the boundary-layer mode of convection should be expected to transport supercooled liquid into the body of the liquid region and thus to cause the experimentally observed supercooling of the liquid region.

Once the mushy layer has become thick enough (always assuming that it has infinite horizontal extent) it must become unstable to the mushy-layer mode. It will do so irrespective of the pre-existence of the boundary-layer mode of instability, though it is quite possible that the boundary-layer mode might trigger a sub-critical instability of the mushy-layer mode. (It can be anticipated that the mushy-layer mode will be subcritically unstable since, in the nonlinear regime, the decrease in solid fraction caused by upflow will result in greater permeability, which is analogous to Bénard convection in a fluid with temperature-dependent viscosity.)

It can be argued (Worster 1986; Kerr *et al.* 1990) that the fluid in the interior of the mushy layer remains very close to the local liquidus temperature, even when kinetic undercooling is significant at the mush–liquid interface, owing to the very large specific surface area of phase boundaries in the dendritic interior. It has been shown further (Worster 1991) that the assumption of equilibrium in the interior of the mushy layer and the difference between thermal and solutal diffusivities cause the fluid emanating from fully developed chimneys to be unsaturated. Thus chimney convection is predicted to maintain the liquid region above the local liquidus and can even cause the temperature of the liquid to increase relative to the liquidus (Worster 1990), in agreement with the experimental observations of Huppert (1990).

The boundary-layer mode of instability depends mainly on the physical properties of the liquid phase, which have similar magnitudes for most aqueous solutions. Therefore, the occurrence of the boundary-layer mode has a similar likelihood in laboratory experiments using aqueous solutions, regardless of the salt being crystallized. Using the criterion discovered in §6 that the boundary-layer mode becomes unstable when $R_{\delta C}$ is greater than about 10, we can deduce that in the transient experiments in which aqueous solutions are cooled at a constant-

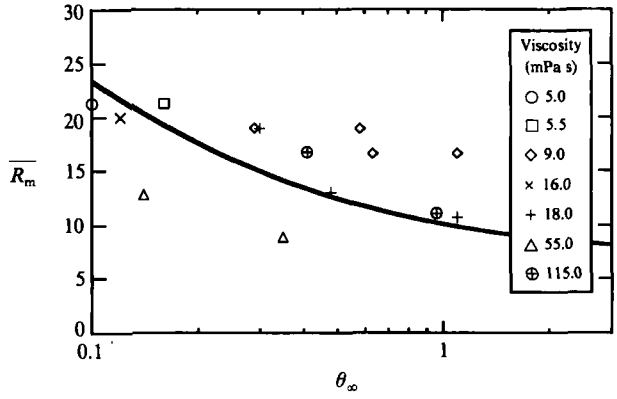

FIGURE 12. The critical Rayleigh number $\overline{R_m}$ as a function of the superheat θ_∞ for parameter values $\mathscr{S} = 5$ and $\mathscr{C} = 20$. The solid line shows the prediction of the linear-stability theory presented in this paper while the data are from experiments by Tait & Jaupart (1992). Different symbols are used to distinguish the different viscosities of the melt used in the experiments.

temperature base the boundary-layer mode will set in once the depth of the mushy layer exceeds about

$$h_0 = \left\{10\frac{\kappa^2\nu}{\beta^* g D}\left[\frac{\Gamma}{T_\infty - T_L(C_0)}\right]\right\}^{\frac{1}{3}}\left[\frac{T_L(C_0)-T_B}{T_\infty - T_L(C_0)}\right],$$

where T_B is the temperature of the cooled base, which gives a value for h_0 in the region of 1 mm for typical parameter values.

The occurrence of the mushy-layer mode is much harder to predict, owing mainly to the uncertainty in the appropriate values of the permeability of the mushy layer. The crystalline morphology varies greatly from one salt to another and this will have a profound influence on the permeability. However, some indication of the relative likelihood of the mushy-layer mode (and hence chimneys) can be gleaned from the results of the present paper. A parameter that varies greatly between the various experiments is the concentration ratio $\mathscr{C}$. In typical experiments with ammonium chloride, for example, $\mathscr{C}$ has a value of about 20. In contrast, the experiment with sodium carbonate reported by Huppert (1990) has a value of $\mathscr{C}$ of about 2. We have seen, in figure 11, that the critical Rayleigh number is extremely sensitive to the value of $\mathscr{C}$ and that systems with higher values of $\mathscr{C}$ are more unstable to the mushy-layer mode and might therefore be expected to be more prone to the formation of chimneys.

The results of recent experiments by Tait & Jaupart (1992) using aqueous solutions of ammonium chloride allowed the authors to estimate critical Rayleigh numbers $\overline{R_m}$ for the onset of the mushy-layer mode of convection. The parameters of their experiments correspond to dimensionless parameters of approximately $\mathscr{C} = 20$ and $\mathscr{S} = 5$, while θ_∞ was varied between about 0.1 and 1.1. In figure 12, the data of Tait & Jaupart (1992) are compared with the predictions of the critical Rayleigh number determined by the present analysis.

It should be borne in mind that the theory is for the steady solidification of a mushy layer at constant speed, whereas the experiments examined time-dependent solidification from a cooled boundary. In addition, Tait & Jaupart (1992) estimated the permeability by applying the Kozeny equation to a regular array of smooth cylinders. The mushy layer, by contrast, is composed of dendritic crystals that have

a larger specific surface area and therefore a lower permeability than the cylinders for a given solid fraction. This effect would have led the authors to overestimate the critical Rayleigh number.

It can be seen that, although there is a fair amount of scatter in the data, they are in good approximate agreement with the theoretical predictions. In particular, the theory and the experiments are consistent in showing the critical value of $\bar{R}_m$ decreasing as θ_∞ increases. This result, which seems counter-intuitive at first, might be explained as follows. When the superheat θ_∞ is large, the density profile is almost linear, whereas the density profile is concave upwards for general values of the superheat. The curvature causes the effective depth over which the density varies to be smaller than the depth of the mushy layer, which will cause the system to be more stable.

This paper has elucidated the nature of the linear convective instabilities that can occur in a mushy layer that is being cooled from below, and the results indicate that attention should focus upon the mushy-layer mode of instability if the initial formation of chimneys is to be understood. This mode can conveniently be studied in the asymptotic limit $D/\kappa \to 0$. Chimneys are intrinsically a finite-amplitude phenomenon, since there is no mechanism for localization of the flow in the linearized system of equations, so there is clearly a need for research into the nonlinear evolution of this system. It is also anticipated that a stability analysis similar to the present one, in addition to allowing predictions of when chimneys might form, will provide constraints on the vigour of convection and the number density of chimneys once they are fully developed. An analysis of this is currently being undertaken.

I am very grateful to S. Tait and C. Jaupart for supplying the data presented in figure 12, to M. Liebman for his help in preparing figures 11 and 12, and to S. H. Davis, H. E. Huppert and R. C. Kerr for their valuable reviews of an earlier draft of this paper. This research was supported by a Research Initiation Grant from the Thermal Systems Program of the National Science Foundation.

REFERENCES

Bear, J. 1988 *Dynamics of Fluids in Porous Media*. Dover.

Chen, F. & Chen, C. F. 1988 Onset of finger convection in a horizontal porous layer underlying a fluid layer. *Trans. ASME* C: *Heat Transfer* **110**, 403–407.

Chen, F. & Chen, C. F. 1991 Experimental study of directional solidification of aqueous ammonium chloride solution. *J. Fluid Mech.* **227**, 567–586.

Copley, S. M., Giamei, A. F., Johnson, S. M. & Hornbecker, M. F. 1970 The origin of freckles in binary alloys. *IMA J. Appl. Maths* **35**, 159–174.

Coriell, S. R., Cordes, M. R., Boettinger, W. J. & Sekerka, R. F. 1980 Convective and interfacial instabilities during unidirectional solidification of a binary alloy. *J. Crystal Growth* **49**, 13–28.

Fowler, A. C. 1985 The formation of freckles in binary alloys. *IMA J. Appl. Maths* **35**, 159–174.

Hellawell, A. 1987 Local convective flows in partially solidified systems. In *Structure and Dynamics of Partially Solidified Systems* (ed. D. E. Loper), pp. 5–22. Martinus Nijhoff.

Huppert, H. E. 1990 The fluid dynamics of solidification. *J. Fluid Mech.* **212**, 209–240.

Huppert, H. E. & Worster, M. G. 1985 Dynamic solidification of a binary melt. *Nature* **314**, 703–707.

Hurle, D. T. J., Jakeman, E. & Wheeler, A. A. 1983 Hydrodynamic stability of the melt during solidification of a binary allow. *Phys. Fluids* **26**, 624–626.

Kerr, R. C., Woods, A. W., Worster, M. G. & Huppert, H. E. 1990 Solidification of an alloy cooled from above. Part 2. Non-equilibrium interfacial kinetics. *J. Fluid Mech.* **217**, 331–348.

NANDAPURKAR, P., POIRIER, D. R., HEINRICH, J. C. & FELICELLI, S. 1989 Thermosolutal convection during dendritic solidification of alloys: Part 1. Linear stability analysis. *Metall. Trans.* **20** B, 711–721.

NG, B. S. & REID, W. H. 1980 On the numerical solution of the Orr–Somerfeld problem: asymptotic initial conditions for shooting methods. *J. Comput. Phys.* **38**, 275–293.

POIRIER, D. R. 1987 Permeability to flow of interdendritic liquid in columnar–dendritic alloys. *Metall. Trans.* **18** B, 245–255.

SARAZIN, J. R. & HELLAWELL, A. 1988 Channel formation in Pb–Sn, Pb–Sb, and Pb–Sn–Sb alloy ingots and comparison with the system NH_4Cl—H_2O. *Metall. Trans.* **19** A, 1861–1871.

TAIT, S. & JAUPART, C. 1992 Compositional convection in a reactive crystalline mush and the evolution of porosity. *J. Geophys. Res.* (submitted).

TURNER, J. S. 1979 *Buoyancy Effects in Fluids.* Cambridge University Press.

WORSTER, M. G. 1986 Solidification of an alloy from a cooled boundary. *J. Fluid Mech.* **167**, 481–501.

WORSTER, M. G. 1990 Structure of a convecting mushy layer. *Appl. Mech. Rev.* **43**, S59–S62.

WORSTER, M. G. 1991 Natural convection in a mushy layer. *J. Fluid Mech.* **224**, 335–359.